Volume 12 | Number 13 | 7 July 2025

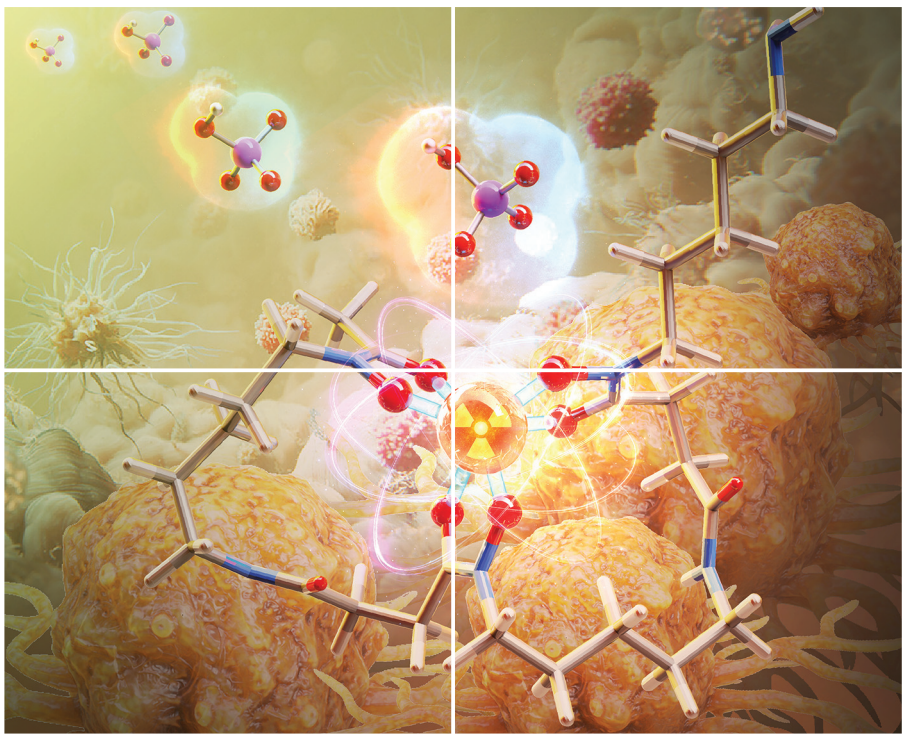

INORGANIC CHEMISTRY

FRONTIERS

CCS 中国化学会 CHINESE CHEMICAL SOCIETY

PEKING UNIVERSITY 1898

ROYAL SOCIETY OF CHEMISTRY

rsc.li/frontiers-inorganic

INORGANIC CHEMISTRY FRONTIERS

RESEARCH ARTICLE

View Article Online
View Journal | View Issue

Cite this: *Inorg. Chem. Front.*, 2025, **12**, 4178

Synergistic coordination in ^{89}Zr–DFO (deferoxamine) complexes: computational and experimental insights into auxiliary ligands†

Jiarui Li, ‡[a,b] Chenghe Ding,‡[c] Yang Gao, *[a,b] Lili Wen,[b] Pingping Zhao,[a] Zhou Lu, [c] Rui Luo,[d] Mingsong Shi, [c] Georg Schreckenbach, *[e] Xiaoan Li *[c,f] and Zhiming Wang [a,b]

Received 31st March 2025,
Accepted 12th April 2025

DOI: 10.1039/d5qi00879d

rsc.li/frontiers-inorganic

This study combines computational and experimental methods to investigate how auxiliary ligands enhance thermodynamic stability in hexacoordinate ^{89}Zr–DFO (deferoxamine) complexes. Strong electrostatic interactions favour HPO_4^{2-} over H_2O, Cl^-, CO_3^{2-} and $C_2O_4^{2-}$, indicating superior stability for advanced medical diagnostics and treatment applications.

The potential applications of the radioisotope ^{89}Zr ($t_{1/2}$ = 78.4 h, β^+ = 22.8%, $E_{\beta^+\max}$ = 901 keV) in medical imaging and therapy have attracted significant attention.[1–11] Deferoxamine (DFO), known for its excellent biocompatibility, is widely used as a hexadentate chelator in clinical and preclinical trials for binding with ^{89}Zr.[1,10–23] However, due to the large ionic radius and octahedral coordination preference of ^{89}Zr,[12,24–37] the Zr^{IV}–DFO hexadentate chelate often experiences *in vivo* demetallation, potentially affecting bone uptake,[28,33,38] bone marrow radiation dose, and nuclear medicine diagnostics precision.[12,31,39–42] To address DFO's incomplete coordination, auxiliary ligands, including water molecules and other anions in the solution, fill vacant coordination sites. Additional research indicates that these auxiliary ligands directly affect the spectroscopic, magnetic, and electronic structure properties of the complex. Moreover, they can alter the oxidation state of the central atom.[43–51] Therefore, a systematic investigation of interactions between $^{89}Zr^{IV}$–DFO complexes and auxiliary ligands not only reveals the essence of these interactions but also emphasizes the crucial role of auxiliary ligands in competing for coordination positions.

Small molecules or ions, with minimal susceptibility to steric repulsion effects, efficiently bind into the first coordination sphere of metal complexes, demonstrating remarkable specificity in these interactions.[45,46,52] As a result, this work systematically characterizes a range of DFO aqueous complexes that may form during the synthesis of ^{89}Zr-labeled chelators,[40,53,54,69] involving tetravalent Zr^{IV} coordinated with both monodentate and bidentate ligands. These auxiliary ligands that form such complexes are commonly present under typical experimental conditions, such as H_2O (solvent) Cl^- (for ion exchange or elution), $C_2O_4^{2-}$ (for complexation), and CO_3^{2-} and HPO_4^{2-} (as buffer components).[55–59,69]

All calculations were performed using density functional theory at the PBE-D3/TZ2P level; solvent effects were incorporated into all calculations using the conductor-like screening solvation model (COSMO), as detailed in Part 1 of ESI.† The study comprehensively assesses thermodynamic stability and intrinsic coordination mechanism through simulations of interactions between auxiliary ligands and Zr^{IV}–DFO complexes. Experimentally, thermodynamic stability sequences were analyzed using radio-thin layer chromatography (radio-TLC) combined with high-performance liquid chromatography (HPLC), as detailed in Part 1 of ESI.† This dual approach elucidates the roles of different auxiliary ligands, providing insights into the coordination dynamics and stability of Zr^{IV}–DFO complexes.

[a]*Institute of Fundamental and Frontier Sciences, University of Electronic Science and Technology of China, Chengdu, Sichuan 611731, China. E-mail: ygaoxs@gmail.com, ygaoxs@uestc.edu.cn*
[b]*Shimmer Center, Tianfu Jiangxi Laboratory, Chengdu 641419, China*
[c]*NHC Key Laboratory of Nuclear Technology Medical Transformation, Mianyang Central Hospital, School of Medicine, University of Electronic Science and Technology of China, Mianyang, Sichuan, 621099, China. E-mail: lixiaoan@sc-mch.cn*
[d]*Department of Nuclear Medicine, Mianyang Central Hospital, Mianyang 621000, China*
[e]*Department of Chemistry, University of Manitoba, Winnipeg, Manitoba R3T 2N2, Canada. E-mail: schrecke@cc.umanitoba.ca*
[f]*Department of Gastroenterology, National Clinical Key Specialty, Mianyang Central Hospital, School of Medicine, University of Electronic Science and Technology of China, Mianyang 621000, China*

†Electronic supplementary information (ESI) available: Method details, eight possible geometrical isomer structures, optimized geometries, geometric parameters, comparison of structural parameters, discussion of the optimized geometry of the aquo complex, complex formation reactions, EDA-NOCV deformation densities of complexes, and Cartesian coordinates. See DOI: https://doi.org/10.1039/d5qi00879d

‡These authors contributed equally to this work.

We studied the eight possible geometric isomers of DFO,[60] where the most stable structure was used for the subsequent studies (Λ-*N*-*cis*, *cis*; see Part 2 of the ESI†). Initially, the Zr^{IV}–DFO complex, atomic plane 1 (green in Fig. 1a), consisting of O atoms from three N–O bonds, and atomic plane 2 (grey in Fig. 1a), consisting of O atoms from three C–O bonds, exhibits a shape reminiscent of a trigonal antiprism (TAP). This arrangement creates additional space for the complementary coordination of auxiliary ligands. Concurrently, Fig. 1b illustrates the octacoordinated structure of Zr^{IV} (see Part 3 of ESI† for details), resembling a square antiprism (SAP). Upon introducing auxiliary ligands (Fig. 1c) into Zr^{IV}–DFO, anionic ligands with high electronegativity (compared to the H_2O ligand) selectively occupy the synergic coordination (SC) 1 and 2 positions within the octahedral coordination sphere (depicted in Fig. 1b). This not only induces an expansion of the first coordination sphere but also leads to an increase in the twist angles ω_1 and ω_2 (see Part 4 of ESI†). These findings imply that the integration of auxiliary ligands may improve the thermodynamic stability of the chelate complex, which has been reported in previous studies.[12,61] Furthermore, the computed bond lengths of the Zr^{IV}–DFO complex closely correspond to previously reported values,[7,12,35,61–63] providing robust validation for the reliability of our methodology (see Part 5 of the ESI†).

Intriguingly, the introduction of water molecules unfolds in a unique way. Occupying the first coordination site, one water molecule impedes subsequent entry due to repulsion from the electron density shield formed by its oxygen atoms and those in DFO.[5,12,24,27,61] Consequently, access to the first coordination layer becomes challenging, and it has also been mentioned in previous literature that there is at least a very tight bound intrabulbar water in the complex of Zr^{IV}–DFO and H_2O,[27,61,64] which is consistent with the formation of a dynamical fluctuating $[Zr^{IV}(DFO)(^{in}H_2O)(^{out}H_2O)]^+$ complex with a relatively 'loose' 7-/8-coordination (see Part 6 of ESI† for details). This inclination facilitates easy exchange between the complex and other solvent-coordinated molecules.

Energy decomposition analysis (EDA) combined with the natural orbitals for chemical valence (NOCV) method was

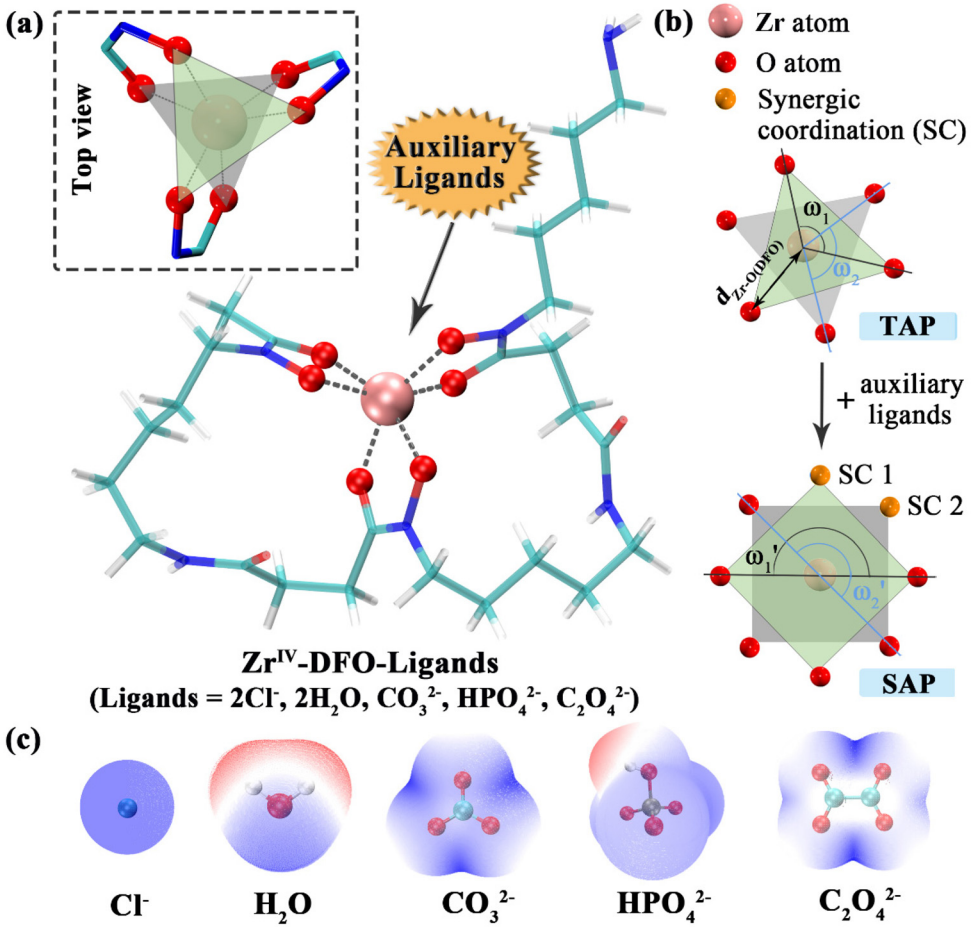

Fig. 1 (a) Optimized geometry of Zr^{IV}–DFO complex and top view of its hexacoordinate sites. (b) Schematic diagram of the transition of Zr^{IV} from hexa-coordinate to octa-coordinate configuration upon the addition of auxiliary ligands. The torsion angles ω_1, ω_2, ω'_1 and ω'_2 define the angles between the corresponding atoms in atomic plane 1 (P1) and atomic plane 2 (P2), respectively. Pink: Zr^{IV}; red: O; orange: synergic coordination (SC) atoms. (c) Electrostatic potential maps of mono- and bidentate ligands. Blue surface: electronegative regions; red surface: electropositive regions.

employed to delve into the chemical bonding properties. The EDA results indicate that the ΔE_{int} values for the anionic (auxiliary ligands) complexes (−232.17 to −288.72 kcal mol^{-1}) are significantly more negative than that of the water molecular complex (−28.79 kcal mol^{-1}), suggesting much stronger interactions (see Part 7 of ESI†). EDA analysis further reveals that electrostatic interaction (ionic bonds) are consistently dominant, with orbital interactions (covalent bonding) as secondary.

The EDA–NOCV calculations allow for a further breakdown of ΔE_{orb} into pairwise orbital interactions (see Fig. 2).[65,66] The results show that the pairwise orbital interactions in the $[Zr^{IV}(DFO)(HPO_4)]^-$ and $[Zr^{IV}(DFO)(CO_3)]^-$ complexes (−45.74 and −46.02 kcal mol^{-1}) are more negative than those in the other complexes, indicating more intense charge transfer. The $\Delta\rho_1$ of $[Zr^{IV}(DFO)(HPO_4)]^-$ and $[Zr^{IV}(DFO)(CO_3)]^-$ complexes primarily involves the donation of electrons from the non-bonding molecular orbitals (NBMO) to the 4d/5s shell orbitals of Zr^{IV}. Similar to actinyl(VI) complexes, small synergistic ligands with partial π bonding significantly influence the coordination, supporting our conclusions.[44] Conversely, the pairwise orbital interactions in $[Zr^{IV}(DFO)(^{in}H_2O)(^{out}H_2O)]^+$ (−15.64 kcal mol^{-1}) are the weakest. Information on other contributions $\Delta\rho$ are given in Part 7 of ESI.†

Further, the relative thermodynamic stabilities of the auxiliary ligands binding to Zr^{IV}–DFO were evaluated through quantum chemical calculations (see Table 1 and Parts 1 and 8 of ESI†). The results from complex formation and ligand substitution reactions indicate that when an anion undergoes synergistic coordination, the thermodynamic stability of the complex exceeds that of the corresponding aqueous complex. Specifically, the sequence is as follows: HPO_4^{2-} (−107.98 kcal mol^{-1}) > CO_3^{2-} (−25.35 kcal mol^{-1}) > $C_2O_4^{2-}$ (−20.65 kcal mol^{-1}) > Cl^- (−13.95 kcal mol^{-1}) > H_2O (≈0 kcal mol^{-1}, due to water acting as both the solute and solvent molecules). Notably, the stability of HPO_4^{2-} binding to Zr^{IV}–DFO is significantly superior. Further theoretical simulations of the complex stability constant (logβ) (see Part 1 of ESI† for the calculation details), yielded results consistent with the thermodynamic stability analysis (see Part 8 of ESI†). To investigate the source of the enhanced stability of the $[Zr^{IV}(DFO)(HPO_4^{2-})]^-$ complex, we analyzed the bonding interactions between the auxiliary ligand and Zr^{IV}–DFO using bond critical points (BCPs) from the quantum theory of atoms in molecules (QTAIM). Our analysis revealed that the HPO_4^{2-} ligand forms additional hydrogen bonds with H atoms on the DFO chain (C–H···O_{86}: 1.96 Å; C–H···O_{87}: 1.98 Å, further details are provided in Part 3 of the ESI†). These additional hydrogen bonds may contribute to the higher thermodynamic stability of the $[Zr^{IV}(DFO)(HPO_4^{2-})]^-$ complex compared to the other complexes. In contrast, for CO_3^{2-}, $C_2O_4^{2-}$, and Cl^-, the interactions with Zr^{IV} are predominantly driven by direct coordination, with little to no hydrogen bonding.

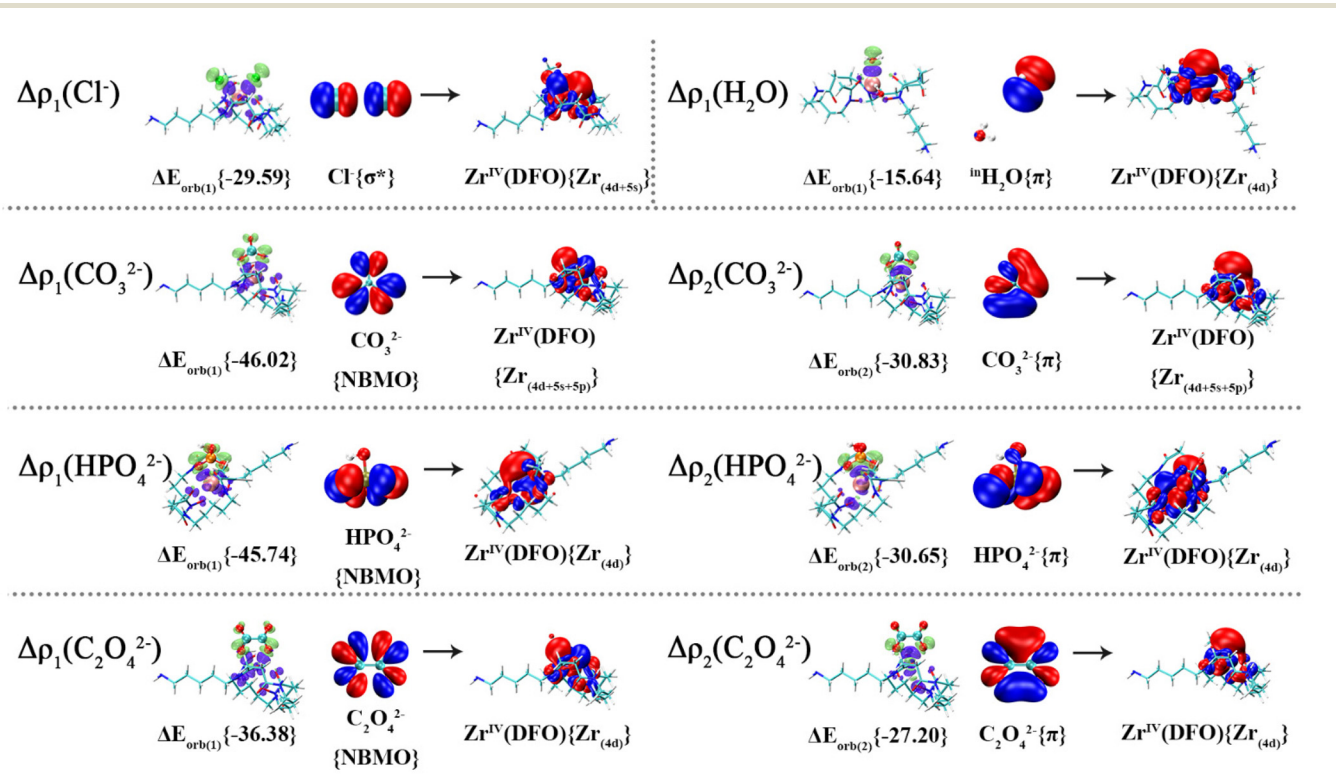

Fig. 2 Plots of EDA–NOCV deformation densities $\Delta\rho$ (isovalue = 0.0015) of the pairwise orbital interactions and the associated fragment molecular orbitals for the different forms of interacting fragments. Energy values for each interaction are enclosed in brackets (kcal mol^{-1}). The charge flow direction is depicted from green to purple. The labels π, NBMO and σ* represent π-bonding, non-bonding and σ-antibonding molecular orbitals, respectively.

Table 1 Gibbs free energy (kcal mol^{-1}) of complex formation reaction and ligand substitution reactions in aqueous solution obtained at PBE-D3/TZ2P levels

Complex formation reactions	Gibbs free energies (ΔG)
$[Zr^{IV}(DFO)]^+ + 2Cl^- \leftrightharpoons [Zr^{IV}(DFO)(Cl)_2]^-$	−13.95
$[Zr^{IV}(DFO)]^+ + CO_3^{2-} \leftrightharpoons [Zr^{IV}(DFO)(CO_3)]^-$	−25.35
$[Zr^{IV}(DFO)]^+ + C_2O_4^{2-} \leftrightharpoons [Zr^{IV}(DFO)(C_2O_4)]^-$	−20.65
$[Zr^{IV}(DFO)]^+ + HPO_4^{2-} \leftrightharpoons [Zr^{IV}(DFO)(HPO_4)]^-$	−107.98
Ligand substitution reactions	**Gibbs free energies ($\Delta\Delta G$)**
$[Zr^{IV}(DFO)(^{in}H_2O)(^{out}H_2O)]^+ + 2Cl^- \leftrightharpoons [Zr^{IV}(DFO)(Cl)_2]^- + 2H_2O$	−13.65
$[Zr^{IV}(DFO)(^{in}H_2O)(^{out}H_2O)]^+ + CO_3^{2-} \leftrightharpoons [Zr^{IV}(DFO)(CO_3)]^- + 2H_2O$	−25.05
$[Zr^{IV}(DFO)(^{in}H_2O)(^{out}H_2O)]^+ + C_2O_4^{2-} \leftrightharpoons [Zr^{IV}(DFO)(C_2O_4)]^- + 2H_2O$	−20.35
$[Zr^{IV}(DFO)(^{in}H_2O)(^{out}H_2O)]^+ + HPO_4^{2-} \leftrightharpoons [Zr^{IV}(DFO)(HPO_4)]^- + 2H_2O$	−107.68
$[Zr^{IV}(DFO)(Cl)_2]^- + CO_3^{2-} \leftrightharpoons [Zr^{IV}(DFO)(CO_3)]^- + 2Cl^-$	−11.40
$[Zr^{IV}(DFO)(Cl)_2]^- + C_2O_4^{2-} \leftrightharpoons [Zr^{IV}(DFO)(C_2O_4)]^- + 2Cl^-$	−6.70
$[Zr^{IV}(DFO)(Cl)_2]^- + HPO_4^{2-} \leftrightharpoons [Zr^{IV}(DFO)(HPO_4)]^- + 2Cl^-$	−94.03
$[Zr^{IV}(DFO)(CO_3)]^- + C_2O_4^{2-} \leftrightharpoons [Zr^{IV}(DFO)(C_2O_4)]^- + CO_3^{2-}$	4.70
$[Zr^{IV}(DFO)(CO_3)]^- + HPO_4^{2-} \leftrightharpoons [Zr^{IV}(DFO)(HPO_4)]^- + CO_3^{2-}$	−82.63
$[Zr^{IV}(DFO)(C_2O_4)]^- + HPO_4^{2-} \leftrightharpoons [Zr^{IV}(DFO)(HPO_4)]^- + C_2O_4^{2-}$	−87.33

To date, numerous studies have shown that the radio-thin layer chromatography (radio-TLC) combined with high-performance liquid chromatography (HPLC) can effectively evaluate the purity, concentration, and *in vitro* stability of [^{89}Zr]Zr-labeled radiopharmaceuticals.[40,55–58,67,68] Based on this, we prepared fresh [^{89}Zr]Zr–DFO–CO_3^{2-} and [^{89}Zr]Zr–DFO–HPO_4^{2-}

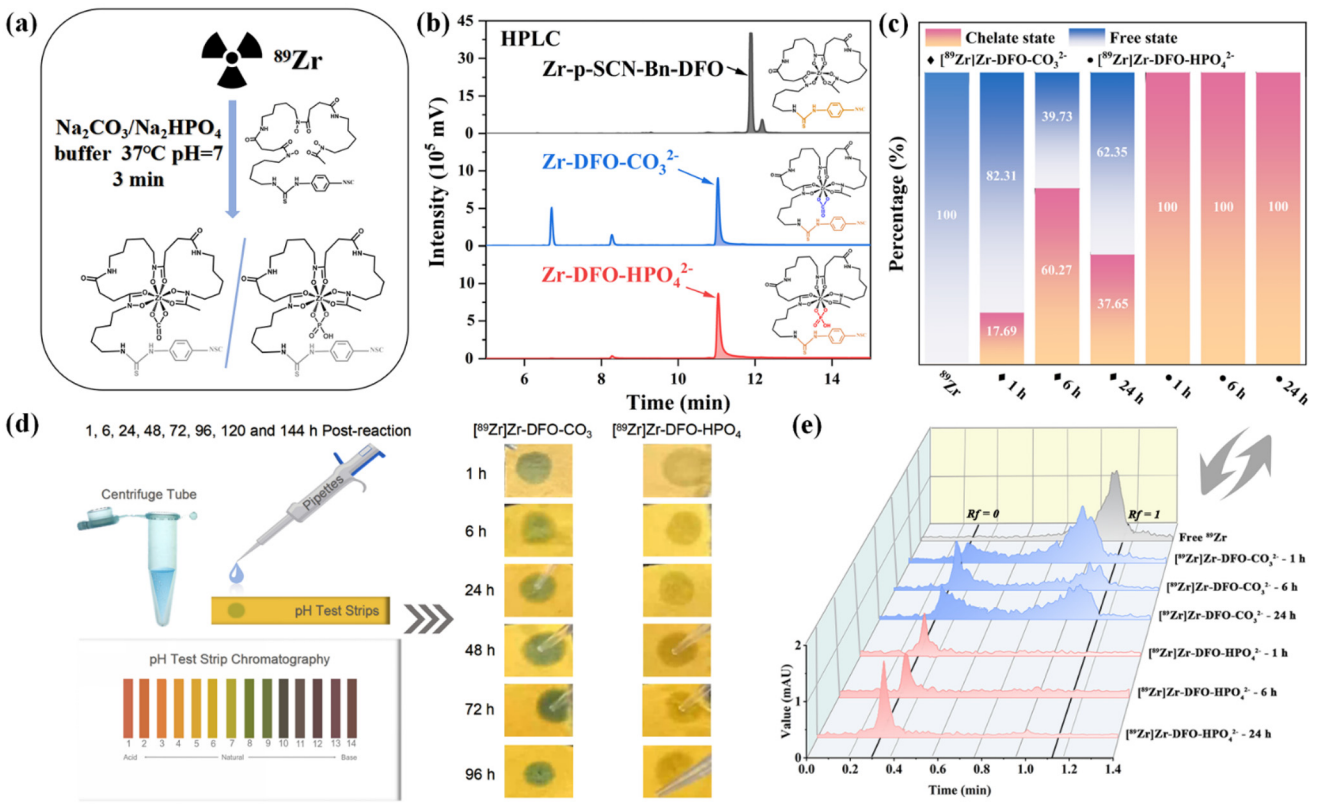

Fig. 3 Labeling and *in vitro* stability of [^{89}Zr]Zr–DFO–ligand complexes. (a) Labeling of DFO and auxiliary ligands (HPO_4^{2-} and CO_3^{2-}) with ^{89}Zr. (b) HPLC results for cold references Zr–DFO–ligand and Zr–DFO. (c) Percentage area plot from radio-TLC analysis of [^{89}Zr]Zr–DFO–ligand complexes. Blue and pink bars represent peak areas corresponding to free and chelated ^{89}Zr, respectively. The square and circle symbols represent [^{89}Zr]Zr–DFO–CO_3^{2-} and [^{89}Zr]Zr–DFO–HPO_4^{2-}. (d) pH changes for [^{89}Zr]Zr–DFO–ligand complexes over 144 hours. (e) Radio-TLC results of [^{89}Zr]Zr–DFO and [^{89}Zr]Zr–DFO–ligand complexes. Gray, blue, and red peaks correspond to free ^{89}Zr, [^{89}Zr]Zr–DFO–CO_3^{2-} and [^{89}Zr]Zr–DFO–HPO_4^{2-} complexes, respectively.

complexes to validate the stability sequence (HPO_4^{2-} > CO_3^{2-}). Initially, ^{89}Zr was produced using a cyclotron, followed by separation, purification, and elution. The radiochemical purity of purified ^{89}Zr exceeded 90% (see Part 9 in ESI†). Alkaline solutions of Na_2CO_3 and Na_2HPO_4, along with *p*-SCN–Bn–DFO, were then added to neutralize the mixture to pH 7. The [^{89}Zr]Zr–DFO–CO_3^{2-} and [^{89}Zr]Zr–DFO–HPO_4^{2-} complexes were successfully prepared by mixing at 37 °C for 60 minutes, as shown in Fig. 3a. A more detailed preparation process is provided in Part 1 of ESI.†

The radiolabeled yield of the complex was measured using radio-TLC (Fig. 3c and e). For complex systems, specific labeled complexes are typically identified by measuring retention factor (R_f) values ranging from 0 to 1. Free ^{89}Zr (unbound $R_f \approx 1$) served as a control (grey area). The [^{89}Zr]Zr–DFO–CO_3^{2-} complex shows two peaks (bound $R_f \approx 0$ and unbound $R_f \approx 1$), while the [^{89}Zr]Zr–DFO–HPO_4^{2-} complex shows only one peak ($R_f \approx 0$). Further analysis revealed that the peak area ratios of the [^{89}Zr]Zr–DFO–CO_3^{2-} system did not increase linearly over 1, 6, and 24 h (Fig. 3c). The observed decrease in chelation content after 6 h suggests several important trends, as shown in our pH data (Fig. 3d): (1) significant pH changes, particularly in the [^{89}Zr]Zr–DFO–CO_3^{2-} system, may be due to the decomposition of carbonic acid. (2) After 6 hours, the pH of the complex solution showed an inverse correlation with the [^{89}Zr]Zr–DFO–CO_3^{2-} complex activity: higher pH values corresponded to lower complex activity. These observations suggest that two main complex forms exist in solution: [^{89}Zr]Zr–DFO and [^{89}Zr]Zr–DFO–CO_3^{2-}. The gradual loss of carbonate ions over time likely contributes to the observed decrease in [^{89}Zr]Zr–DFO–CO_3^{2-} complexation.

On the other hand, a small amount of $ZrCl_4$ and alkaline solutions (Na_2CO_3 and Na_2HPO_4) were reacted with excess DFO in water for 60 min under neutral conditions to prepare the nonradioactive Zr–DFO, Zr–DFO–CO_3^{2-}, and Zr–DFO–HPO_4^{2-} complexes at room temperature. The peaks in HPLC correspond to individual components, identified by their retention time. The results indicated that the retention times of Zr–DFO, Zr–DFO–CO_3^{2-}, and Zr–DFO–HPO_4^{2-} were 11.90, 11.03, and 11.04 minutes, respectively, confirming the identity of each complex (Fig. 3b). These finding highlight HPO_4^{2-}'s superior complexation capacity (thermodynamic stability) with ^{89}Zr–DFO over time. In addition, at 37 °C, [^{89}Zr]Zr–DFO–CO_3^{2-} and [^{89}Zr]Zr–DFO–HPO_4^{2-} were stable in human serum over 7 days. The results are shown in Part 10 of ESI.† In summary, the thermodynamic stability of ^{89}Zr–DFO complexes was rigorously evaluated *via* radio-TLC and HPLC, conclusively demonstrating that the [^{89}Zr(DFO)HPO_4]$^-$ complex exhibits superior stability compared to other complexes, consistent with theoretical predictions discussed above.

Conclusions

In summary, intermolecular electrostatic interactions, specifically ionic bonding, play a crucial role in determining the character, such as the structure and thermodynamic stability, of the complexes. Both theoretical and experimental evidence confirm that HPO_4^{2-} significantly improves the stability of complexes through its unique coordination pattern and hydrogen bonding interactions compared to alternative ligands such as CO_3^{2-}, showing good radiolabelling efficiency and *in vitro* stability (7 day integrity in serum). Considering the impact of different coordinating molecules on the octahedral complex of ^{89}Zr and practical factors such as the thermal stability of the complexes and subsequent modifications, we believe that this study will advance the development of highly stable chelating agents for ^{89}Zr, supporting precise quantitative applications of biomarkers such as immune positron emission tomography (PET) and prostate-specific membrane antigen (PSMA).

Author contributions

Yang Gao, Georg Schreckenbach and Xiaoan Li: conceptualization, funding acquisition, experimental support, review and editing; Jiarui Li and Chenghe Ding: investigation, methodology, writing – original draft, software, visualization, data curation and experimental test; Lili Wen, Pingping Zhao, Zhou Lu, Rui Luo, Mingsong Shi and Zhiming Wang: investigation, discussion and data curation.

Data availability

The ESI† includes method details of theory and experiments, possible geometrical isomer structures, optimized geometries, geometric parameters, bond critical point calculations, comparison with previous structural parameters, discussion of the optimized geometry of the aqueous complex, metal ligand complexation reactions, stability constant, EDA–NOCV deformation densities of complexes, characterization of radiochemical purity, and *in vitro* stability comparisons. The geometrical coordinates involved in this work are shown in the XYZ file.

Conflicts of interest

There are no conflicts to declare.

Acknowledgements

The authors would like to thank Prof. Caterina F. Ramogida for helpful discussions. YG acknowledges the support of the Science and Technology Department of Sichuan Province (2024NSFSC0294), the Central Guidance for Local Science and Technology Development Funds Project (2024ZYD0161), the NHC Key Laboratory of Nuclear Technology Medical Transformation (Mianyang Central Hospital) (Grant No. 2022HYX002, 2022HYX003), and the Tianfu Jiangxi Laboratory (No. TFJX-ZD-2024-005). XL acknowledges the support of the NHC Key Laboratory of Nuclear Technology Medical

Transformation (Mianyang Central Hospital) (Grant No. 2021HYX010), the Science and Technology Department of Sichuan Province (2023YFS0470), and the Mianyang Science and Technology Bureau (Minyang Science and Technology Program, Grant No. 2022ZYDF085). GS acknowledges funding from the Natural Sciences and Engineering Council of Canada, NSERC (Discovery Grant, RGPIN-2023-04922). CD acknowledges the support of the Health Commission of Sichuan Province (Popularization of application project, Grant No. 21PJ182).

References

1 M. A. Deri, B. M. Zeglis, L. C. Francesconi and J. S. Lewis, PET imaging with ^{89}Zr: From radiochemistry to the clinic, *Nucl. Med. Biol.*, 2013, **40**, 3–14.
2 G. Fischer, U. Seibold, R. Schirrmacher, B. Wängler and C. Wängler, ^{89}Zr, a radiometal nuclide with high potential for molecular imaging with PET: Chemistry, applications and remaining challenges, *Molecules*, 2013, **18**, 6469–6490.
3 Y. W. Jauw, C. W. Menke-van der Houven van Oordt, O. S. Hoekstra, N. H. Hendrikse, D. J. Vugts, J. M. Zijlstra, M. C. Huisman and G. A. van Dongen, Immuno-positron emission tomography with zirconium-89-labeled monoclonal antibodies in oncology: What can we learn from initial clinical trials?, *Front. Pharmacol.*, 2016, **7**, 131.
4 D. J. Vugts, G. W. M. Visser and G. A. M. S. van Dongen, ^{89}Zr-PET radiochemistry in the development and application of therapeutic monoclonal antibodies and other biologicals, *Curr. Top. Med. Chem.*, 2013, **13**, 446–457.
5 J. P. Holland, The radiochemistry of zirconium, in *Handbook of Radiopharmaceuticals*, John Wiley & Sons, Ltd, 2020.
6 M. Patra, S. Klingler, L. S. Eichenberger and J. P. Holland, Simultaneous photoradiochemical labeling of antibodies for immuno-positron emission tomography, *iScience*, 2019, **13**, 416–431.
7 M. A. Deri, S. Ponnala, P. Kozlowski, B. P. Burton-Pye, H. T. Cicek, C. Hu, J. S. Lewis and L. C. Francesconi, *p*-SCN-Bn-HOPO: A Superior Bifunctional Chelator for ^{89}Zr ImmunoPET, *Bioconjugate Chem.*, 2015, **26**, 2579–2591.
8 D. R. Beckford-Vera, R. R. Flavell, Y. Seo, E. Martinez-Ortiz, M. Aslam, C. Thanh, E. Fehrman, M. Pardons, S. Kumar, A. N. Deitchman, V. Ravanfar, B. Schulte, I. W. K. Wu, T. Pan, J. D. Reeves, C. C. Nixon, N. S. Iyer, L. Torres, S. E. Munter, T. Hyunh, C. J. Petropoulos, R. Hoh, B. L. Franc, L. Gama, R. A. Koup, J. R. Mascola, N. Chomont, S. G. Deeks, H. F. VanBrocklin and T. J. Henrich, First-in-human immunoPET imaging of HIV-1 infection using ^{89}Zr-labeled VRC01 broadly neutralizing antibody, *Nat. Commun.*, 2022, **13**, 1219.
9 J. P. Holland, M. J. Evans, S. L. Rice, J. Wongvipat, C. L. Sawyers and J. S. Lewis, Annotating MYC status with ^{89}Zr-transferrin imaging, *Nat. Med.*, 2012, **18**, 1586–1591.
10 L. Melendez-Alafort, G. Ferro-Flores, L. De Nardo, B. Ocampo-García and C. Bolzati, Zirconium immune-complexes for PET molecular imaging: Current status and prospects, *Coord. Chem. Rev.*, 2023, **479**, 215005.
11 U. Seibold, B. Wängler and C. Wängler, Rational Design, Development, and Stability Assessment of a Macrocyclic Four-Hydroxamate-Bearing Bifunctional Chelating Agent for ^{89}Zr, *ChemMedChem*, 2017, **12**, 1555–1571.
12 J. P. Holland, V. Divilov, N. H. Bander, P. M. Smith-Jones, S. M. Larson and J. S. Lewis, ^{89}Zr-DFO-J591 for immunoPET of prostate-specific membrane antigen expression in vivo, *J. Nucl. Med.*, 2010, **51**, 1293–1300.
13 G. W. Severin, J. W. Engle, T. E. Barnhart and R. J. Nickles, 89Zr radiochemistry for positron emission tomography, *Med. Chem.*, 2011, **7**, 389–394.
14 D. Bellotti and M. Remelli, Deferoxamine B: A natural, excellent and versatile metal chelator, *Molecules*, 2021, **26**, 3255.
15 B. M. Zeglis, J. L. Houghton, M. J. Evans, N. Viola-Villegas and J. S. Lewis, Underscoring the influence of inorganic chemistry on nuclear imaging with radiometals, *Inorg. Chem.*, 2014, **53**, 1880–1899.
16 E. K. Sarbisheh, A. K. Salih, S. J. Raheem, J. S. Lewis and E. W. Price, A high-denticity chelator based on desferrioxamine for enhanced coordination of zirconium-89, *Inorg. Chem.*, 2020, **59**, 11715–11727.
17 J. P. Holland, E. Caldas-Lopes, V. Divilov, V. A. Longo, T. Taldone, D. Zatorska, G. Chiosis and J. S. Lewis, Measuring the pharmacodynamic effects of a novel Hsp90 inhibitor on HER2/*neu* expression in mice using ^{89}Zr-DFO-trastuzumab, *PLoS One*, 2010, **5**, e8859.
18 J. R. Dilworth and S. I. Pascu, The chemistry of PET imaging with zirconium-89, *Chem. Soc. Rev.*, 2018, **47**, 2554–2571.
19 S. Tendler, M. P. Dunphy, M. Agee, J. O'Donoghue, R. G. Aly, N. J. Choudhury, A. Kesner, A. Kirov, A. Mauguen, M. K. Baine, H. Schoder, W. A. Weber, N. Rekhtman, S. K. Lyashchenko, L. Bodei, M. J. Morris, J. S. Lewis, C. M. Rudin and J. T. Poirier, Imaging with [^{89}Zr]Zr-DFO-SC16.56 anti-DLL3 antibody in patients with high-grade neuroendocrine tumours of the lung and prostate: a phase 1/2, first-in-human trial, *Lancet Oncol.*, 2024, **25**, 1015–1024.
20 M. Savastano, C. Bazzicalupi, G. Ferraro, E. Fratini, P. Gratteri and A. Bianchi, Tales of the Unexpected: The Case of Zirconium(IV) Complexes with Desferrioxamine, *Molecules*, 2019, **24**, 2098.
21 J. N. Tinianow, H. S. Gill, A. Ogasawara, J. E. Flores, A. N. Vanderbilt, E. Luis, R. Vandlen, M. Darwish, J. R. Junutula, S.-P. Williams and J. Marik, Site-specifically ^{89}Zr-labeled monoclonal antibodies for ImmunoPET, *Nucl. Med. Biol.*, 2010, **37**, 289–297.
22 I. Verel, G. W. Visser, R. Boellaard, M. Stigter-van Walsum, G. B. Snow and G. A. van Dongen, ^{89}Zr immuno-PET: comprehensive procedures for the production of ^{89}Zr-labeled monoclonal antibodies, *J. Nucl. Med.*, 2003, **44**, 1271–1281.

23 M. Li, S. Wang, Q. Kong, X. Cheng, H. Yan, Y. Xing, X. Lan and D. Jiang, Advances in macrocyclic chelators for positron emission tomography imaging, *View*, 2023, **4**, 20230042.

24 M. Patra, A. Bauman, C. Mari, C. A. Fischer, O. Blacque, D. Häussinger, G. Gasser and T. L. Mindt, An octadentate bifunctional chelating agent for the development of stable zirconium-89 based molecular imaging probes, *Chem. Commun.*, 2014, **50**, 11523–11525.

25 M. A. Deri, S. Ponnala, B. M. Zeglis, G. Pohl, J. J. Dannenberg, J. S. Lewis and L. C. Francesconi, Alternative chelator for ^{89}Zr radiopharmaceuticals: Radiolabeling and evaluation of 3,4,3-(LI-1,2-HOPO), *J. Med. Chem.*, 2014, **57**, 4849–4860.

26 L. Allott, C. Da Pieve, J. Meyers, T. Spinks, D. M. Ciobota, G. Kramer-Marek and G. Smith, Evaluation of DFO-HOPO as an octadentate chelator for zirconium-89, *Chem. Commun.*, 2017, **53**, 8529–8532.

27 K. L. Summers, E. K. Sarbisheh, A. Zimmerling, J. J. H. Cotelesage, I. J. Pickering, G. N. George and E. W. Price, Structural characterization of the solution chemistry of zirconium(IV) desferrioxamine: A coordination sphere completed by hydroxides, *Inorg. Chem.*, 2020, **59**, 17443–17452.

28 A. K. Salih, M. Dominguez Garcia, S. J. Raheem, W. K. Ahiahonu and E. W. Price, DFO-Km: A modular chelator as a new chemical tool for the construction of zirconium-89-based radiopharmaceuticals, *Inorg. Chem.*, 2023, **62**, 20806–20819.

29 C. Buchwalder, C. Rodríguez-Rodríguez, P. Schaffer, S. K. Karagiozov, K. Saatchi and U. O. Häfeli, A new tetrapodal 3-hydroxy-4-pyridinone ligand for complexation of ^{89}zirconium for positron emission tomography (PET) imaging, *Dalton Trans.*, 2017, **46**, 9654–9663.

30 J. P. Holland, Predicting the thermodynamic stability of zirconium radiotracers, *Inorg. Chem.*, 2020, **59**, 2070–2082.

31 J. P. Holland and N. Vasdev, Charting the mechanism and reactivity of zirconium oxalate with hydroxamate ligands using density functional theory: Implications in new chelate design, *Dalton Trans.*, 2014, **43**, 9872–9884.

32 M. Savastano, F. Boscaro and A. Bianchi, Metal Coordination Properties of a Chromophoric Desferrioxamine (DFO) Derivative: Insight on the Coordination Stoichiometry and Thermodynamic Stability of Zr^{4+} Complexes, *Molecules*, 2022, **27**, 184.

33 S. Heskamp, R. Raavé, O. Boerman, M. Rijpkema, V. Goncalves and F. Denat, ^{89}Zr-Immuno-Positron Emission Tomography in Oncology: State-of-the-Art ^{89}Zr Radiochemistry, *Bioconjugate Chem.*, 2017, **28**, 2211–2223.

34 N. B. Bhatt, D. N. Pandya and T. J. Wadas, Recent Advances in Zirconium-89 Chelator Development, *Molecules*, 2018, **23**, 638.

35 F. Guérard, Y. S. Lee, R. Tripier, L. P. Szajek, J. R. Deschamps and M. W. Brechbiel, Investigation of Zr (IV) and ^{89}Zr(IV) complexation with hydroxamates: progress towards designing a better chelator than desferrioxamine B for immuno-PET imaging, *Commun. Chem.*, 2013, **49**, 1002–1004.

36 F. d'Orchymont and J. P. Holland, A rotaxane-based platform for tailoring the pharmacokinetics of cancer-targeted radiotracers, *Chem. Sci.*, 2022, **13**, 12713–12725.

37 M. Brandt, J. Cowell, M. L. Aulsebrook, G. Gasser and T. L. Mindt, Radiolabelling of the octadentate chelators DFO* and oxoDFO* with zirconium-89 and gallium-68, *J. Biol. Inorg. Chem.*, 2020, **25**, 789–796.

38 Y. Toporivska and E. Gumienna-Kontecka, The solution thermodynamic stability of desferrioxamine B (DFO) with Zr(IV), *J. Inorg. Biochem.*, 2019, **198**, 110753.

39 A. K. Salih, S. J. Raheem, M. D. Garcia, W. K. Ahiahonu and E. W. Price, Design, synthesis, and evaluation of DFO-Em: A modular chelator with octadentate chelation for optimal zirconium-89 radiochemistry, *Inorg. Chem.*, 2022, **61**, 20964–20976.

40 J. P. Holland, Y. Sheh and J. S. Lewis, Standardized methods for the production of high specific-activity zirconium-89, *Nucl. Med. Biol.*, 2009, **36**, 729–739.

41 W. E. Meijs, H. J. Haisma, R. P. Klok, F. B. van Gog, E. Kievit, H. M. Pinedo and J. D. Herscheid, Zirconium-labeled monoclonal antibodies and their distribution in tumor-bearing nude mice, *J. Nucl. Med.*, 1997, **38**(1), 112–118.

42 M. T. Ma, L. K. Meszaros, B. M. Paterson, D. J. Berry, M. S. Cooper, Y. Ma, R. C. Hider and P. J. Blower, Tripodal tris(hydroxypyridinone) ligands for immunoconjugate PET imaging with $^{89}Zr^{4+}$: comparison with desferrioxamine-B, *Dalton Trans.*, 2015, **44**, 4884–4900.

43 Y. Gao, A. Jennifer G, E. Varathan and G. Schreckenbach, Understanding the coordination chemistry of Am^{III}/Cm^{III} in the DOTA cavity: Insights from energetics and electronic structure theory, *Inorg. Chem.*, 2023, **62**, 3229–3237.

44 Y. Gao, E. Varathan, P. Grover and G. Schreckenbach, Computational characterization of Ac^{III}-DOTA complexes in aqueous solution, *Inorg. Chem.*, 2021, **60**, 6971–6975.

45 G. T. Kent, G. Wu and T. W. Hayton, Synthesis and Crystallographic Characterization of the Tetravalent Actinide-DOTA Complexes [AnIV(k^8-DOTA)(DMSO)] (An = Th, U), *Inorg. Chem.*, 2019, **58**, 8253–8256.

46 G. Dovrat, M. C. Illy, C. Berthon, A. Lerner, M. H. Mintz, E. Maimon, R. Vainer, Y. Ben-Eliyahu, Y. Moiseev, P. Moisy, A. Bettelheim and I. Zilbermann, On the aqueous chemistry of the U^{IV}-DOTA complex, *Chem. – Eur. J.*, 2020, **26**, 3390–3403.

47 A. R. Khabibullin, A. Karolak, M. M. Budzevich, M. L. McLaughlin, D. L. Morse and L. M. Woods, Structure and properties of DOTA-chelated radiopharmaceuticals within the ^{225}Ac decay pathway, *MedChemComm*, 2018, **9**, 1155–1163.

48 Y. Gao, P. Grover and G. Schreckenbach, Stabilization of hydrated Ac^{III} cation: The role of superatom states in actinium-water bonding, *Chem. Sci.*, 2021, **12**, 2655–2666.

49 B. L. McNeil and C. F. Ramogida, From cyclotrons to chromatography and beyond: a guide to the production

and purification of theranostic radiometals, *Chem. Soc. Rev.*, 2024, **53**, 10409–10449.

50 A. Hu and J. J. Wilson, in *Radiopharmaceutical Therapy*, ed. L. Bodei, J. S. Lewis and B. M. Zeglis, Springer International Publishing, Cham, 2023, pp. 123–144. DOI: 10.1007/978-3-031-39005-0_6.

51 C. Ramogida and E. Price, in *Positron Emission Tomography: Methods and Protocols*, ed. T. H. Witney and A. J. Shuhendler, Springer US, New York, NY, 2024, pp. 65–101. DOI: 10.1007/978-1-0716-3499-8_6.

52 M. Audras, L. Berthon, C. Berthon, D. Guillaumont, T. Dumas, M. C. Illy, N. Martin, I. Zilbermann, Y. Moiseev, Y. Ben-Eliyahu, A. Bettelheim, S. Cammelli, C. Hennig and P. Moisy, Structural Characterization of Am(III)- and Pu(III)-DOTA Complexes, *Inorg. Chem.*, 2017, **56**, 12248–12259.

53 M. Chomet, M. Schreurs, M. J. Bolijn, M. Verlaan, W. Beaino, K. Brown, A. J. Poot, A. D. Windhorst, H. Gill, J. Marik, S. Williams, J. Cowell, G. Gasser, T. L. Mindt, G. A. M. S. van Dongen and D. J. Vugts, Head-to-head comparison of DFO* and DFO chelators: Selection of the best candidate for clinical ^{89}Zr-immuno-PET, *Eur. J. Nucl. Med. Mol. Imaging*, 2020, **48**, 694–707.

54 R. Raavé, G. Sandker, P. Adumeau, C. B. Jacobsen, F. Mangin, M. Meyer, M. Moreau, C. Bernhard, L. Da Costa, A. Dubois, V. Goncalves, M. Gustafsson, M. Rijpkema, O. Boerman, J. C. Chambron, S. Heskamp and F. Denat, Direct comparison of the in vitro and in vivo stability of DFO, DFO* and DFOcyclo* for ^{89}Zr-immunoPET, *Eur. J. Nucl. Med. Mol. Imaging*, 2019, **46**, 1966–1977.

55 A. Larenkov, V. Bubenschikov, A. Makichyan, M. Zhukova, A. Krasnoperova and G. Kodina, Preparation of Zirconium-89 Solutions for Radiopharmaceutical Purposes: Interrelation Between Formulation, Radiochemical Purity, Stability and Biodistribution, *Molecules*, 2019, **24**, 1534.

56 N. Li, Z. Yu, T. T. Pham, P. J. Blower and R. Yan, A generic ^{89}Zr labeling method to quantify the in vivo pharmacokinetics of liposomal nanoparticles with positron emission tomography, *Int. J. Nanomed.*, 2017, **12**, 3281–3294.

57 A. Bansal, M. K. Pandey, Y. E. Demirhan, J. J. Nesbitt, R. J. Crespo-Diaz, A. Terzic, A. Behfar and T. R. DeGrado, Novel ^{89}Zr cell labeling approach for PET-based cell trafficking studies, *EJNMMI Res.*, 2015, **5**, 19.

58 D. Ulmert, M. J. Evans, J. P. Holland, S. L. Rice, J. Wongvipat, K. Pettersson, P.-A. Abrahamsson, P. T. Scardino, S. M. Larson, H. Lilja, J. S. Lewis and C. L. Sawyers, Imaging Androgen Receptor Signaling with a Radiotracer Targeting Free Prostate-Specific Antigen, *Cancer Discovery*, 2012, **2**, 320–327.

59 T. E. Wuensche, S. Lyashchenko, G. A. M. S. van Dongen and D. Vugts, Good practices for 89Zr radiopharmaceutical production and quality control, *EJNMMI Radiopharm. Chem.*, 2024, **9**, 40.

60 B. Borgias, A. D. Hugi and K. N. Raymond, Isomerization and solution structures of desferrioxamine B complexes of aluminum(3+) and gallium(3+), *Inorg. Chem.*, 1989, **28**, 3538–3545.

61 E. E. Racow, J. J. Kreinbihl, A. G. Cosby, Y. Yang, A. Pandey, E. Boros and C. J. Johnson, General approach to direct measurement of the hydration state of coordination complexes in the gas phase: Variable temperature mass spectrometry, *J. Am. Chem. Soc.*, 2019, **141**, 14650–14660.

62 P. Jewula, J. C. Berthet, J. C. Chambron, Y. Rousselin, P. Thuéry and M. Meyer, Synthesis and Structural Study of Tetravalent (Zr^{4+}, Hf^{4+}, Ce^{4+}, Th^{4+}, U^{4+}) Metal Complexes with Cyclic Hydroxamic Acids, *Eur. J. Inorg. Chem.*, 2015, **2015**, 1529–1541.

63 F. Guérard, M. Beyler, Y. S. Lee, R. Tripier, J. F. Gestin and M. W. Brechbiel, Investigation of the complexation of ^{nat}Zr(iv) and ^{89}Zr(iv) by hydroxypyridinones for the development of chelators for PET imaging applications, *Dalton Trans.*, 2017, **46**, 4749–4758.

64 A. Guillou, A. Ouadi and J. P. Holland, Heptadentate chelates for ^{89}Zr-radiolabelling of monoclonal antibodies, *Inorg. Chem. Front.*, 2022, **9**, 3071–3081.

65 R. B. Woodward and R. Hoffmann, The conservation of orbital symmetry, *Angew. Chem., Int. Ed. Engl.*, 1969, **8**, 781–853.

66 K. Fukui, *Theory of orientation and Stereoselection*, Springer Verlag, Berlin, 1975.

67 N. B. Bhatt, D. N. Pandya, J. Xu, D. Tatum, D. Magda and T. J. Wadas, Evaluation of macrocyclic hydroxyisophthalamide ligands as chelators for zirconium-89, *PLoS One*, 2017, **12**, e0178767.

68 J. N. Tinianow, D. N. Pandya, S. L. Pailloux, A. Ogasawara, A. N. Vanderbilt, H. S. Gill, S. P. Williams, T. J. Wadas, D. Magda and J. Marik, Evaluation of a 3-hydroxypyridin-2-one (2,3-HOPO) Based Macrocyclic Chelator for $^{89}Zr^{4+}$ and Its Use for ImmunoPET Imaging of HER2 Positive Model of Ovarian Carcinoma in Mice, *Theranostics*, 2016, **6**, 511–521.

69 Zirconium oxalate solution is suitable for complexation reactions involving DFO ligand, but oxalic acid is highly toxic and may cause acute renal failure. To remove oxalic acid, the cartridge can be flushed with a large amount of water and exchanged with chloride ions. In addition, Na_2CO_3 may be used to adjust the pH to 7 during the experiment. H_2O, Cl^-, $C_2O_4^{2-}$ and CO_3^{2-} are all planar structures, and HPO_4^{2-} was studied to explore the effect of non-planar small molecules on ^{89}Zr–DFO hexadentate chelate.